



The Effect of Water Vapor on NiO Formation by Ni–Cr Alloys at 650 °C (HTCPM Focus Issue, FNS-111)

Chengyang Jiang^{1,2} · Jianqiang Zhang² · David J. Young¹

Received: 30 May 2021 / Revised: 30 May 2021 / Accepted: 1 June 2021 /
Published online: 29 June 2021

© The Author(s), under exclusive licence to Springer Science+Business Media, LLC, part of Springer Nature 2021

Abstract

Exposure of Ni–Cr alloys containing 5–30 wt% Cr to Ar-20O₂ and Ar-20O₂-20H₂O at 650 °C produced an external NiO layer, internal chromium oxidation and an intermediate zone of NiO + Cr₂O₃. The NiO layer growth rate decreased with increasing alloy Cr content. Addition of water vapor to dry O₂ changed the NiO grain structure from equiaxed-shaped to columnar-shaped. In pure water vapor, a thin external NiO layer was formed above a layer of unoxidized metallic Ni, with an IOZ beneath. Water vapor effects on NiO formation are discussed in terms of different mechanisms whereby the volume increase in the IOZ is accommodated.

Keywords Ni–Cr alloy · NiO · Water vapor · Growth kinetics · Morphology

Introduction

Nickel-based alloys have been used as construction materials for high-temperature components in supercritical (SC) and ultra-supercritical (USC) fossil fuel power plants within the temperature range of 650–800 °C [1–3], due to their superior corrosion resistance and creep strength. A slow growing, homogeneous and continuous oxide scale, chromia or alumina, is preferred, to protect the underlying alloys from attack in aggressive environments and achieve extended service life.

✉ David J. Young
d.young@unsw.edu.au

Chengyang Jiang
cyjjiang1991@hotmail.com

Jianqiang Zhang
j.q.zhang@unsw.edu.au

¹ School of Materials Science and Engineering, UNSW, Sydney, Australia

² Corrosion and Protection Division, Shenyang National Laboratory for Materials Science, Northeastern University, Wenhua Road 3#, Shenyang 110819, China

The oxidation behavior of various model Ni–Cr alloys in air and oxygen has been studied extensively [4–7]. The effect of water vapor on the oxidation behavior of Ni–Cr alloys has also been reported and found to be complex and dependent upon the oxidizing environments. Some authors found the chromia scale thickness to be reduced in wet O₂ and air compared with those formed in the corresponding dry gases [6, 8]. Others [9, 10] reported that chromia scales exhibited higher growth rates in Ar–H₂O and Ar–H₂–H₂O than in Ar–O₂. On the other hand, several studies reported a duplex morphology of Cr₂O₃ with equiaxed, basaltic or columnar grains, which can be strongly influenced by the nature of the oxidizing atmosphere and in particular the presence of water vapor [11, 12]. Latu-Romain et al. [13] found that the inner layer always exhibits n-type semiconduction, while the outer layer shifts from n-type to insulator and finally to p-type semiconduction when oxygen partial pressure is increased. Thus, the effect of water vapor on oxidation behavior is related to oxygen partial pressure.

Many reports of the water vapor effects have focused mainly on external chromia scale formation [6, 8] and oxygen permeability in alloy [14, 15]. In contrast, the water vapor effect on NiO formation of Ni–Cr alloys has received little attention, although studies of water vapor reaction with pure Ni or dilute Ni–Cr alloys are available in the literature [16, 17].

In the present work, the oxidation behavior of binary Ni–Cr alloys was studied at 650 °C in three different atmospheres: Ar–20O₂, Ar–20O₂–20H₂O, and Ar–20H₂O (vol%). In Ar–20H₂O, the equilibrium oxygen partial pressure in Ar–20H₂O is 8.0×10^{-9} atm. The aim was to elucidate the effect of water vapor on NiO outer layer formation in terms of kinetics, morphology and scale structure. The intention was to relate these phenomena to what was happening to the underlying alloy.

Experimental Procedures

Model alloys, Ni-5, 10, 15, 20, 25, 30Cr (nominal composition, all in wt%), were fabricated by arc-melting high-purity metals Ni (99.95%) and Cr (99.995%) under a protective Ar-5%H₂ gas atmosphere, using a non-consumable tungsten electrode. The resulting button-shaped cast alloy ingots, ~20 mm diameter and 4 mm thick, were annealed at 1100 °C for 50 h in a flowing Ar-5%H₂ gas for homogenization and then slowly furnace-cooled. Annealed alloy grains were coarse and irregular: from 1.0 to 1.5 mm for Ni-5Cr and Ni-10Cr, 0.5–1.0 mm for Ni-15Cr and Ni-20Cr, and 0.2–0.5 mm for Ni-25Cr and Ni-30Cr alloys. Alloy compositions were checked by energy-dispersive X-ray spectroscopy and confirmed to be close to their nominal compositions, as reported before, 5.2 wt% Cr for Ni-5Cr and 25.1 wt% for Ni-25Cr [18]. Analysis by X-ray diffraction confirmed that all test alloys were single-phase austenite.

Rectangular test samples of approximate dimensions (10–14) mm × (6–8) mm × (0.8–1.3) mm were cut from the homogenized ingots, ground to a 1200-grit finish, polished down to a 3-μm finish and then electropolished in 15% hydrochloric acid to remove the work-hardened subsurface region. All samples were ultrasonically cleaned in ethanol immediately before reaction.

Isothermal corrosion experiments were carried out in a vertical furnace equipped with a quartz tubular reactor, except that the exposures in Ar-20H₂O were performed in a horizontal furnace equipped with an alumina tubular reactor. In both cases, alloys were exposed to a flowing gas mixture with a linear flow rate of 2 cm/s at a total pressure of 1 atm at 650 °C. Each exposure experiment was continuous for the predetermined time.

Individual gas flows of Ar and O₂ were regulated by mass flow controllers. Wet gases of controlled water vapor partial pressure were generated by passing the gas through a thermostatted water saturator. The demineralized water in contact with the gas mixture was set at a temperature producing an excess of water vapor. This excess water was subsequently condensed by cooling the wet gas in a distillation column at the temperature corresponding to the required water vapor content. Before reaction, the reactor was purged with pure argon for 1 h. Before oxidation, the samples hung in the cold zone of the furnace tube to avoid selective oxidation of chromium during heating. Then, a preheated furnace was moved to position the samples in its hot zone to commence an exposure, and the reaction gas introduced. After exposure, the samples were cooled in the cold zone of the furnace tube.

Specimen weights were measured using an analytical balance (Mettler Toledo XP205) with an accuracy of 0.01 mg. Cross sections of reacted samples were characterized by optical microscopy (OM) and scanning electron microscopy (SEM; Hitachi S3400). The outer-layer (OL) thickness was measured at 10 different locations in cross-sectional images to gain an average value and standard deviation. For some selected areas, transmission electron microscopy (TEM; Tecnai G2 F30) equipped with energy-dispersive X-ray spectroscopy (EDS) was used for detailed analyses. TEM samples were prepared by using focused ion beam (FIB, FEI xT Nova Nanolab 200) milling from places of interest on reacted samples.

Results

NiO Growth Kinetics

Our early work [18] has indicated that in dry/wet O₂, a three-layered structure was formed by alloys containing 5–25Cr: an outer NiO layer (OL), an inner oxide layer of (NiO+Cr₂O₃) and an internal oxidation zone (IOZ). However, in water vapor alone, all alloys underwent internal oxidation, nickel metal expulsion and external NiO formation. Figure 1 shows OL growth kinetics in dry/wet O₂ and water vapor. It is observed that in Ar-20O₂ (Fig. 1a), the NiO growth rates were generally rapid for Ni-5Cr and Ni-10Cr alloys, but decreased somewhat for alloys with Cr levels of 15–25 wt%. Adding water vapor to O₂ (Fig. 1b) reduced the total OL thickness, and the OL growth rates decreased gradually with increasing alloy Cr content. The NiO growth kinetics in Ar-20H₂O followed a similar pattern to that in dry/wet O₂, but the thickness was further reduced. These OL thicknesses can be generally approximated by parabolic kinetics, which is expressed by the equation:

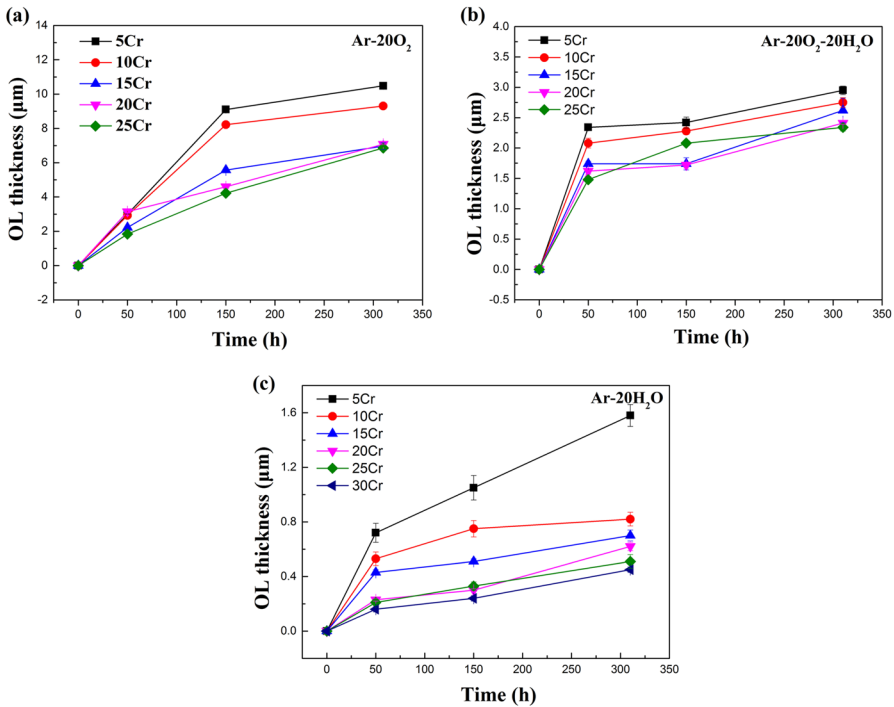


Fig. 1 Outer-layer NiO growth kinetics in (a) Ar-20O₂, b Ar-20O₂-20H₂O and c Ar-20H₂O at 650 °C

$$X^2 = 2k_p t \quad (1)$$

where X is the thickness of NiO after time t , and k_p the parabolic rate constant. Rate constants calculated according to Eq. (1) are listed in Table 1. The Ni-30Cr alloy was excluded in dry/wet O₂ due to its formation of a continuous chromia layer with discontinuous outer NiO islands.

As is obvious, NiO is formed fastest in dry O₂ but slowest in water vapor alone. In all three gases, NiO growth rates decrease with increasing alloy Cr concentration, the effect being smaller in wet oxygen.

Table 1 Parabolic rate constants (k_p (10⁻³ μm² h⁻¹)) of OL growth kinetics

Ni–Cr Alloy	Ni-5Cr	Ni-10Cr	Ni-15Cr	Ni-20Cr	Ni-25Cr	Ni-30Cr
Ar-20O ₂	190 ± 40	150 ± 35	80 ± 11	79 ± 5	75 ± 7	/
Ar-20O ₂ -20H ₂ O	12 ± 4	10 ± 3	9 ± 2	8 ± 2	8 ± 2	/
Ar-20H ₂ O	7.9 ± 0.4	2.0 ± 0.6	1.4 ± 0.2	1.2 ± 0.2	0.8 ± 0.1	0.6 ± 0.1

Morphological Evolution of NiO

Alloy cross sections after exposure in Ar-20O₂, Ar-20O₂-20H₂O and Ar-20H₂O for 310 h at 650 °C have been described elsewhere [18]. The development with time of these reaction product structures is examined here, using Ni-20Cr as an example. Backscattered electron (BSE)-SEM cross-sectional images showing the evolution of oxide morphology in Ar-20O₂ are presented in Fig. 2a–c. It is seen that a three-layered structure has been formed at the alloy surface after corrosion for only 50 h. This structure persisted through longer exposures, all three layers growing thicker with time. The outer layer was identified by diffraction

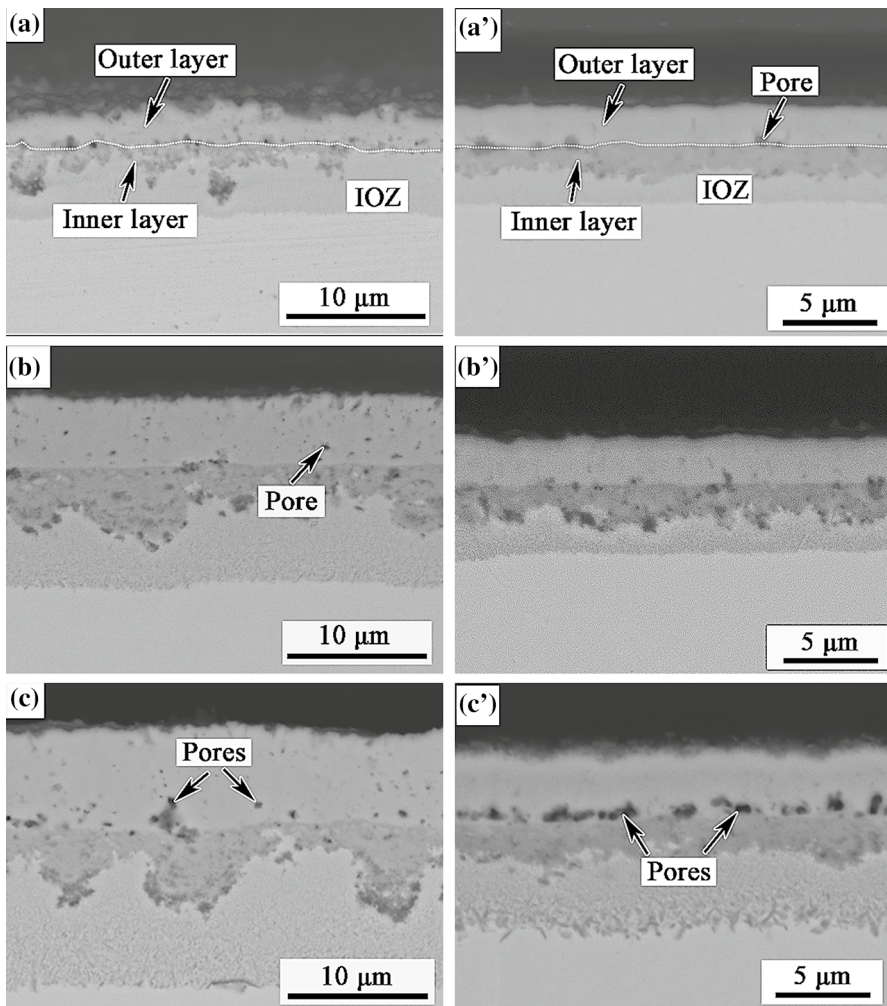


Fig. 2 BSE-SEM cross sections of Ni-20Cr alloy after reaction in Ar-20O₂ (left column) and Ar-20O₂-20H₂O (right column) at 650 °C for different times: (a, a') 50 h, (b, b') 150 h and (c, c') 310 h

(see below) as NiO and confirmed by EDS to be essentially pure (55.0 Ni-45.0 O, at.%). Small pores were observed at the interface of outer and inner layers. As reaction time increased, additional pores were found throughout the NiO layer.

Figure 2a–c shows BSE-SEM cross-sectional images revealing the morphological evolution of Ni-20Cr reaction products in Ar-20O₂-20H₂O. The pattern of NiO outer layer was generally similar to that in Ar-20O₂. There were two distinct differences; however, the NiO thickness was much smaller than that formed in dry O₂, and the pores in this layer appeared mainly near the interface between outer and inner layers.

The BSE-SEM cross-sectional images of Ni-20Cr after reaction in Ar-20H₂O (Fig. 3) reveal a very different product morphology. After 50-h reaction in pure water vapor, a thin external NiO layer containing metallic Ni was formed above an internal oxidation zone (Fig. 3a). Distinct layers of metal and oxide developed subsequently, and their thicknesses increased with time. Large Ni nodules were clearly seen at some locations (Fig. 3b). The metallic Ni developed into a continuous layer, covered by a dense NiO layer, above which grew complex whiskery oxide structures (Fig. 3c).

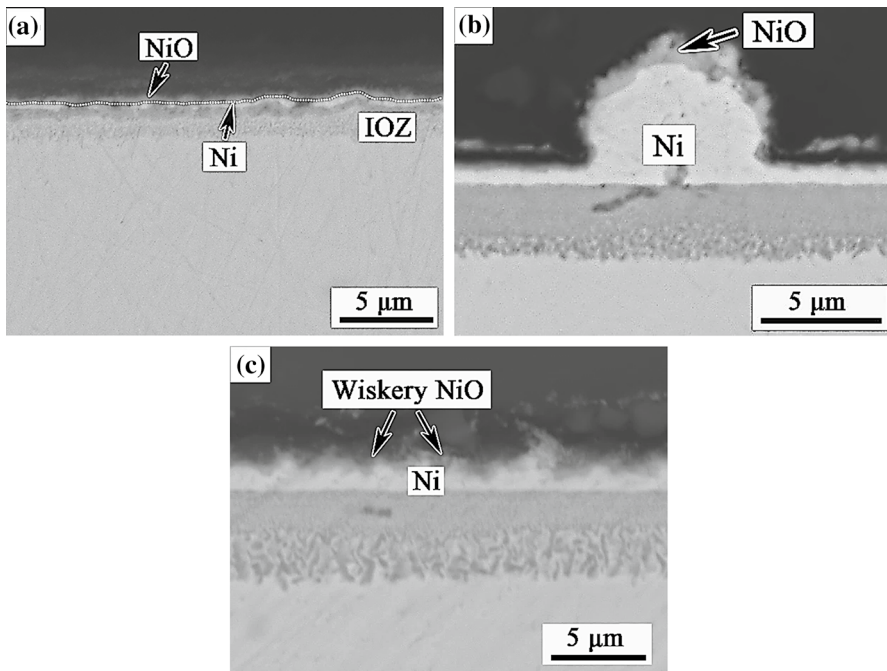


Fig. 3 BSE-SEM cross sections of Ni-20Cr alloy after reaction in Ar-20H₂O at 650 °C for different times: **a** 50 h, **b** 150 h and **c** 310 h

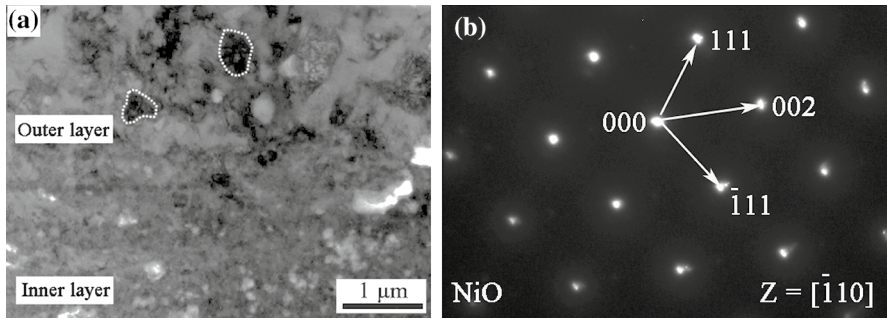


Fig. 4 **a** Cross-sectional bright-field image and **b** SAD patterns of outer layer of Ni-20Cr after reaction in Ar-20O₂ for 310 h. Selected oxide grains outlined with dotted lines

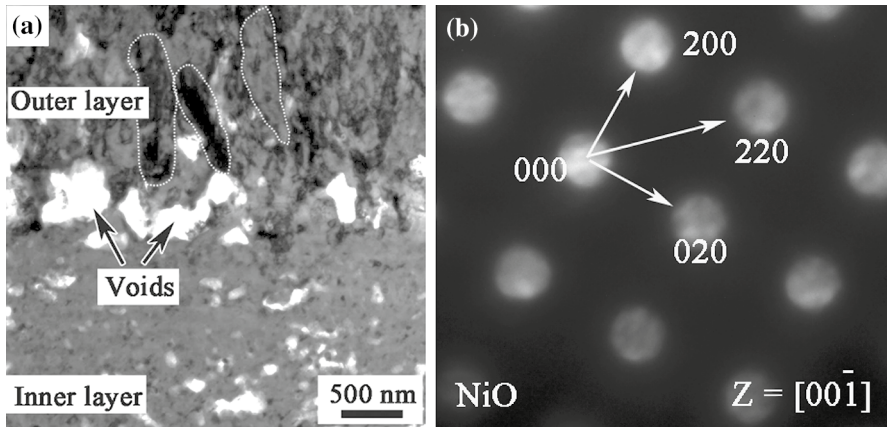


Fig. 5 **a** Cross-sectional bright-field image and **b** SAD patterns of outer layer of Ni-20Cr after reaction in Ar-20O₂-20H₂O for 310 h. Selected oxide grains outlined with dotted lines

NiO Microstructure

A bright-field (BF)-TEM cross-sectional image in Fig. 4a shows the outer oxide scale layers developed on Ni-20Cr reacted for 310 h in dry O₂. It reveals relatively coarse (about 200 nm) equiaxed grains and a fine-grained inner layer. This layer was confirmed as NiO by selected area diffraction (SAD) (Fig. 4b). A bright-field TEM image for the oxide scale on Ni-20Cr reacted in wet O₂ for 310 h in Fig. 5a shows outer layer grains to be columnar-shaped. SAD patterns (Fig. 5b) confirmed the layer to be NiO.

Discussion

Effect of Water Vapor on NiO Growth Kinetics

In order to explain different growth kinetics of NiO developed in wet and dry O₂ gases, pure Ni samples (≥ 99.7 wt% confirmed by EDS) were exposed to the two atmospheres for 310 h at 650 °C [18]. The corresponding weight gains after 150 h of reaction were 0.55 mg/cm² in dry O₂ and 0.04 mg/cm² in wet O₂, respectively, consistent with corresponding values of k_p found in the current study (Table 1) for NiO growth on Ni–Cr alloys. It is seen that the oxidation of pure Ni is consistently slower in wet O₂ than in dry O₂ at 650 °C. This result is similar to that found by Essuman et al. [8], who reported that pure Ni exposed in water vapor had a reduced oxidation rate compared with that in oxygen. One of the reasons why nickel reacts very slowly in water vapor is the preferential adsorption of H₂O by NiO [19–21]. Water vapor reacts very slowly, owing to the non-acidic p-type oxide nature of NiO [19]. However, there is also a change in the transport processes within the oxide which, at this temperature, are in the main confined to grain boundaries.

Nickel oxide growth is usually considered to occur via outward diffusion of Ni through the NiO scale because Ni diffusion is much faster (by 2 orders of magnitude) than that of oxygen [16]. Recession of the metal surface is accommodated largely, but not completely, by deformation of the oxide. In addition, as nickel diffuses outwards to react rapidly with oxygen, vacancies are injected into the metal, where they coalesce and are encapsulated in the nickel oxide, accounting for its porosity. However in the case of wet O₂ and water vapor reactions, water vapor-derived species occupy grain boundary sites. Their nature is as yet undefined, but presumably involve hydrogen. The presence of hydroxyls or water molecules on grain boundaries impedes outward nickel diffusion, but facilitates inward oxygen transport. This accounts for the observed inward growth of the NiO [18] and implies that vacancies are injected into the metal more slowly or not at all. The latter effect is important in the case of Ni–Cr reactions, where Cr is oxidized internally.

Effect of Water Vapor on NiO Morphology

Alloy reaction morphologies after reaction in pure water vapor are significantly different from those developed in dry O₂: a pure nickel layer remains beneath the external NiO. This can be attributed to the reduced oxidation rate of nickel in H₂O, coupled with the continuing ejection of metal from the IOZ.

The formation of Cr₂O₃ precipitates in the IOZ is accompanied by a volume expansion. For one mole of alloy, the volume change, ΔV , is given by

$$\Delta V = N_{\text{Cr}} V_{\text{CrO}_{1.5}} + N_{\text{Ni}} V_{\text{Ni}} - V_{\text{Alloy}} \quad (2)$$

where N_i and V_i are mole fractions and molar volumes of the indicated species. Approximating $V_{\text{Ni}} \approx V_{\text{Alloy}}$, one obtains

$$\Delta V = N_{Cr}(V_{CrO_{1.5}} - V_{Alloy}) \tag{3}$$

Setting $V_{Alloy} = 6.8 \text{ cm}^3$ and $V_{CrO_{1.5}} = 14.6 \text{ cm}^3$ leads to the evaluation for Ni-20Cr alloy ($N_{Cr} = 0.22$) of $\Delta V/V_{Alloy} = 0.25$, a large volume.

Space can be made available for the internal oxide in two ways: dilation of the entire zone or removal of a substantial amount of nickel from the IOZ. The observation that NiO forms mainly as an external, single-phase layer suggests the latter process is more important. Removal of nickel can be accomplished by its diffusion in the metal phase, that is by creep, or its diffusion as cations within a reaction product NiO layer. If the growth of NiO occurs via outward cation diffusion, metal is consumed at the NiO layer underside, injecting vacancies into the metal.

If this process is fast enough, space is provided for the increased oxide volume in the IOZ. If the NiO layer growth is even faster, then additional oxidation of the nickel metal matrix of the IOZ occurs, as seen in the reaction with dry O_2 (Fig. 2). However, if vacancies are not injected fast enough at the NiO/Ni interface, compressive stresses in the IOZ increase, leading to the expulsion of metal (Fig. 3). To investigate these issues, quantitative image analysis [22] was used to measure the relevant volumes in reaction zones formed by Ni-20Cr.

Figure 6a and c shows measured volumes per unit surface area of internal oxidation zones and oxidized Ni developed in the three gases. Here V_{IOZ} is the volume of

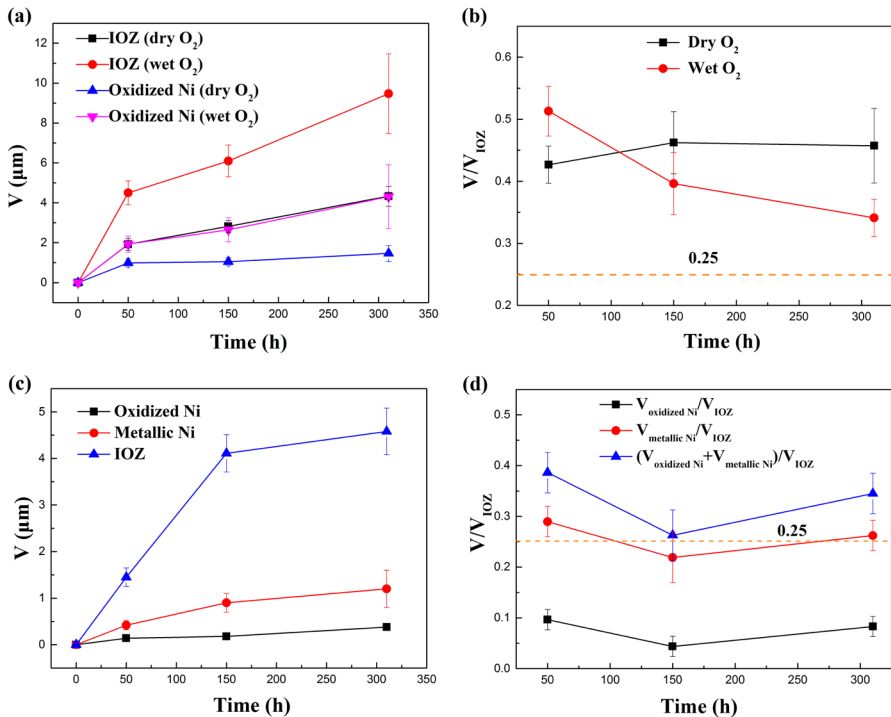


Fig. 6 Evolution with time of volume per unit Ni-20Cr alloy surface area of indicated reaction products, as defined in text: **a** and **b** for dry and wet O_2 ; **c** and **d** for pure water vapor

IOZ per unit alloy surface, assumed to equal the volume of corresponding alloy undergoing internal oxidation; $V_{\text{oxidized Ni}}$ is the equivalent volume of Ni above the external surface and present as oxide. The measured volume of outer NiO was transformed to $V_{\text{oxidized Ni}}$ by multiplying with $\frac{V_{\text{Ni}}}{V_{\text{NiO}}}$ ($V_{\text{NiO}} = 11.11 \text{ cm}^3$). The volume of Ni expelled to external surface, but unoxidized, per unit alloy surface is denoted by $V_{\text{metallic Ni}}$. Pore volumes were excluded.

For the volume increase in the IOZ to be eliminated by outward Ni expulsion requires that $V_{\text{oxidized Ni}} \geq \Delta V$ and $V_{\text{oxidized Ni}}/V_{\text{IOZ}} \geq \Delta V/V_{\text{Alloy}}$. Figure 6b shows that $V_{\text{oxidized Ni}}/V_{\text{IOZ}}$ remained above $\Delta V/V_{\text{Alloy}} = 0.25$ during the entire reaction in the dry and wet O_2 gases, showing that the volume expansion resulting from internal oxidation is accommodated by external NiO layer formation in these cases. This result agrees qualitatively with the relatively flat NiO/IOZ interface, with no metallic nickel formation.

In contrast, Fig. 6d shows the value of $V_{\text{oxidized Ni}}/V_{\text{IOZ}}$ obtained in pure water vapor was well below the requirement of 0.25. As a result, the volume change in the IOZ cannot be accommodated by nickel oxidation. Stress relief within the IOZ cannot thereby be fully achieved. Instead, additional metallic Ni is forced to the external surface. As seen in Fig. 6d, the value of $(V_{\text{oxidized Ni}} + V_{\text{metallic Ni}})/V_{\text{IOZ}} \geq 0.25$. Thus, stress in the IOZ is in this case relieved by Ni transport in the metallic phase..

Nickel oxide layer growth in dry and wet O_2 is fast enough to consume Ni in amounts sufficient to make space for internal Cr_2O_3 precipitates. The growth mechanism of the NiO is critical. The outward Ni diffusion through the oxide creates space for the internal precipitation process by vacancy injection. In contrast, NiO growth in pure water vapor is not only slower, but inward oxygen transport through the NiO is more important [18]. As a result, far fewer vacancies are formed at the oxide/Ni interface, volume expansion accompanying internal oxidation cannot in this case be completely compensated, and space is made available by the ejection of additional Ni metal.

The dissociation of oxidant species has been proposed to be the rate-controlling step for oxide whisker growth, and the faster dissociation of water vapor at dislocation emergent sites promotes whisker formation [23]. This effect is more obvious at lower temperatures. The current experimental results are consistent with this view, which accounts for whiskery NiO growth in pure water vapor.

Effect of Water Vapor on NiO Scale Structure

It is inferred that the microstructure and texture of NiO were affected by the presence of water vapor [24]. Auchi et al. [25] found that water vapor significantly affected the morphology and scale structure of NiO. A duplex NiO scale with a powder-like outer and dense inner NiO layer developed when the Ni was oxidized in atmospheres containing water vapor. The grain size of the dense inner NiO layer was much smaller than that formed in dry atmospheres. Similarly, Hayashi et al. [26] reported that the NiO scale formed in air + H_2O was duplex in structure with outer porous and inner dense layers. The outer porous layer consisted of fine powder-like NiO particles. In the current work, the results shown in Figs. 5a and 6a indicated

that water vapor did change NiO scale structure, from equiaxial to columnar grain. Clarifying the underlying mechanisms requires further study.

Conclusions

A series of model Ni–Cr alloys containing 5–30 wt% Cr were reacted in Ar-20O₂, Ar-20O₂-20H₂O and Ar-20H₂O at 650 °C, and the effects of water vapor on external NiO layer formation, growth kinetics, morphology and scale structure were investigated.

Addition of water vapor to oxygen did not change the NiO morphology, but slowed the NiO growth, accounting for both the thinner NiO layer and its reduced porosity.

In the dry and wet O₂, an external NiO layer of appreciable thickness grew via outward Ni diffusion. This process consumes metal and creates space to accommodate the internal oxide precipitates in the underlying alloy.

In contrast, in pure water vapor, a thin film of NiO developed on Ni nodules/layers at the surface of alloy because inward oxygen transport through NiO is more important. In this case, volume increase resulting from internal oxidation of Cr cannot be fully compensated and additional metallic Ni expulsion results.

Water vapor changed the NiO microstructure, from equiaxed grains in dry O₂ to columnar grains in wet O₂.

Acknowledgements The authors would like to thank the Australian Research Council for financial support under its Discovery Project Scheme. The first author is greatly thankful for scholarship support from the China Scholarship Council (CSC).

References

1. J. P. Shingledecker and G. M. Pharr, *Journal of Materials Engineering and Performance*. **22**, (2), 2013 (454–462).
2. S. J. Patel, J. J. deBarbadillo, B. A. Baker, and R. D. Gollihue, *Procedia Engineering*. **55**, 2013 (246–252).
3. F. Abe, *Engineering*. **1**, (2), 2015 (211–224).
4. G. M. Ecer and G. H. Meier, *Oxidation of Metals*. **13**, (2), 1979 (119–158).
5. K. P. R. Reddy, J. L. Smialek, and A. R. Cooper, *Oxidation of Metals*. **17**, (5), 1982 (429–449).
6. J. Zurek, D. J. Young, E. Essuman, M. Hänsel, H. J. Penkalla, L. Niewolak, and W. J. Quadakkers, *Materials Science and Engineering. A*. **477**, (1), 2008 (259–270).
7. N. Mu, K. Y. Jung, N. M. Yanar, G. H. Meier, F. S. Pettit, and G. R. Holcomb, *Oxidation of Metals*. **78**, (3–4), 2012 (221–237).
8. E. Essuman, G. H. Meier, J. Zurek, M. Haensel, T. Norby, L. Singheiser, and W. J. Quadakkers, *Corrosion Science*. **50**, (6), 2008 (1753–1760).
9. P. Berthod, L. Aranda, S. Mathieu, and M. Vilasi, *Oxidation of Metals*. **79**, (5–6), 2013 (517–527).
10. D. Simon, B. Gorr, and H. J. Christ, *Oxidation of Metals*. **87**, (3–4), 2017 (417–429).
11. A. Holt and P. Kofstad, *Solid State Ionics*. **69**, 1994 (137–143).
12. K. Arnold, G. Tatlock, C. Kenel, A. Colella, and P. Matteazzi, *Materials at. High Temperature*. **5**, 2017 (1–10).
13. L. Latu-Romain, Y. Parsa, S. Mathieu, M. Vilasi, A. Galerie, and Y. Wouters, *Corrosion Science*. **126**, 2017 (238–246).

14. P. Guo, J. Zhang, D. J. Young, and C. H. Konrad, *Oxidation of Metals*. **83**, (3–4), 2015 (223–235).
15. A. Prillieux, D. Jullian, J. Zhang, D. Monceau, and D. J. Young, *Oxidation of Metals*. **87**, (3–4), 2017 (273–283).
16. C. K. Kim and L. W. Hobbs, *Oxidation of Metals*. **47**, (1–2), 1997 (69–89).
17. S. Chevalier, F. Desserrey, and J. Larpin, *Oxidation of Metals*. **64**, (3–4), 2005 (219–234).
18. C. Jiang, Y. Xie, C. Kong, J. Zhang, and D. J. Young, *Corrosion Science*. **174**, 2020 (108801).
19. A. Galerie, Y. Wouters, and M. Caillet, *Materials Science Forum*. **369–372**, 2001 (231–238).
20. C. Anghel, E. Hornlund, G. Hultquist, and M. Limback, *Applied Surface Science*. **233**, (1–4), 2004 (392–401).
21. J. P. Abellan, T. Olszewski, G. H. Meier, L. Singheiser, and W. J. Quadakkers, *International Journal of Materials Research*. **101**, (2), 2010 (287–299).
22. T. J. Collins, *Biotechniques*. **43**, 2007 (25–30).
23. S. R. J. Saunders, M. Monteiro, and F. Rizzo, *Progress in Materials Science*. **53**, (5), 2008 (775–837).
24. J.-H. Ahn, B.-J. Kim, J.-G. Kim, H.-J. Kim, G.-W. Hong, H.-G. Lee, J.-M. Yoo, and H. Pradeep, *Physica C*. **445–448**, 2006 (620–624).
25. M. Auchi, S. Hayashi, K. Toyota, and S. Ukai, *Oxidation of Metals*. **78**, (1–2), 2012 (51–61).
26. S. Hayashi, S. Narita, and T. Narita, *Oxidation of Metals*. **74**, (1–2), 2010 (33–47).

Publisher's Note Springer Nature remains neutral with regard to jurisdictional claims in published maps and institutional affiliations.